RSC Advances

PAPER

View Article Online
View Journal | View Issue

Cite this: *RSC Adv.*, 2021, **11**, 37426

Mechanistic insight of structural and optical properties of BiOCl in the presence of CNTs and investigating photodegradation of phenol by BiOCl/CNT composites

Nikita Sharma,[ab] Bence Veres,[a] Pranjal Dhiman,[c] Zsolt Pap, *[ad] Kornélia Baán,[a] Seema Garg [c] and Klara Hernadi *[ae]

In this work, we have synthesized composites of BiOCl with carbon nanotubes (CNTs) *via* a hydrothermal method. Different compositions of CNTs were used to study their influence on the physicochemical properties of BiOCl. Based on the interesting results obtained, various significant correlations were made. This study explored how use of CNTs and different hydrothermal crystallization conditions can influence the photocatalytic activity of composites. The CNTs have an impact on the primary crystallite size and morphology of BiOCl. Also, a higher degree of crystallization was obtained in the case of samples containing CNTs. However, in some cases, the synthesis parameters such as high temperature and longer duration also promoted crystallinity in BiOCl/CNT samples. Further, the samples were investigated for their photocatalytic activity to study the photodegradation of RhB and phenol, as model pollutants, under visible and UV light, respectively. The maximum degradation efficiency of 83% for RhB under visible light and almost 40% for phenol under UV light was obtained using BiOCl/CNT composites. Surprisingly, pure BiOCl showed higher performance for the removal of both the pollutants. This is why some comparisons and correlations between the structural and optical properties of BiOCl and CNTs were made. Finally, this study illustrates how a nanostructure like conductive multiwalled carbon nanotubes can sometimes have detrimental effects on the overall photocatalytic properties of a photocatalyst like BiOCl under certain conditions. Therefore, understanding the synergy between physico-chemical properties of BiOCl and nanostructured-modifiers like CNTs could help in designing a photocatalyst system which could benefit wastewater treatment.

Received 18th September 2021
Accepted 14th November 2021

DOI: 10.1039/d1ra07003g

rsc.li/rsc-advances

1. Introduction

Bismuth oxyhalides (BiOX, X = Cl, Br, I) are a relatively new class of visible light active photocatalyst and show a narrow band gap energy, except for BiOCl which has a wider band gap energy.[1] They have a unique layered structure that plays a significant role in extending their light-harvesting ability (from the UV to visible region).[2] There has been a tremendous amount of research devoted to BiOX after the first study of BiOCl concerning the photodegradation of methyl orange in 2006 by Zhang *et al.*[3] The applications cover a broad spectrum in the field of photocatalytic energy conversion and environmental remediation, such as hydrogen production by solar water splitting,[4] indoor-gas purification,[5] photocatalytic wastewater treatment,[6] photodegradation of pesticides[7] and other volatile organic compounds (VOC)[8] and nitrogen fixation.[9] All BiOX crystallizes into tetragonal matlockite structure which consists of Bi_2O_2 slabs interleaved by double halogen atom slabs forming a layered structure.

BiOCl is one of the novel and promising candidates among other BiOXs. However, BiOCl has a wide band gap (~3.2–3.4 eV) which is quite close to TiO_2 (*e.g.*: ~3.0–3.2 eV). This popular photocatalyst also has a wide band gap, therefore, such photocatalysts are UV-active.[1] Nevertheless, dye-sensitized BiOCl showed good response for the photodegradation of RhB under visible light.[10] The removal of dyes is widely reported and does not seems to be as challenging as is the case for pollutants like phenol, salicylic acid or oxalic acid *etc.*

[a]*Department of Applied and Environmental Chemistry, University of Szeged, H–6720 Rerrich Béla 1, Szeged, Hungary. E-mail: hernadi@chem.u-szeged.hu; pzsolt@chem.u-szeged.hu*

[b]*Advanced Materials and Intelligent Technologies Higher Education and Industrial Cooperation Centre, University of Miskolc, H-3515 Miskolc, Hungary*

[c]*Department of Chemistry, Amity Institute of Applied Sciences, Amity University, Sector-125, Noida, U. P. 201313, India*

[d]*Nanostructured Materials and Bio-Nano-Interfaces Centre, Institute for Interdisciplinary Research on Bio-Nano-Sciences, Babeş–Bolyai University, Treboniu Laurian 42, Cluj-Napoca, RO400271, Romania*

[e]*Institute of Physical Metallurgy, Metal Forming and Nanotechnology, University of Miskolc, HU-3515 Miskolc-Egyetemváros, C/1 108, Miskolc, Hungary*

A number of factors are known to influence the photocatalytic response of the semiconductor material, such as synthesis parameters, structural, morphological and optical properties, pH, source of light and its intensity and so on. Most of the work found in literature focuses on enhancing the photocatalytic activity of the material and very few studies have reported the fundamental correlations between the performance of photocatalyst and its properties. This is a very important area to study as it gives the background information about the behavior of the material and how certain parameters can influence its properties. Not only this, the prior knowledge of correlations between its properties like structural or optical, with the photocatalytic behavior of the semiconductor would help the researchers in designing the novel photocatalysts with the desired characteristics. One such work was carried out by our research group that studied the effect of solvothermal synthesis conditions (temperature and time) on morphology and crystallinity of BiOX and their impact on the photocatalytic activity.[11] Likewise, other study by Qian *et al.* reports the synergistic effect between the magnetic core Fe_3O_4 that facilitated the interfacial charge transfer process and core shell of BiOI.[12] The present study was also intended to fulfill such gaps since majority of the studies are concerned on modifying the morphological or structural aspects of the photocatalyst which includes modification with the shape and size of the nanomaterials by using certain shape-tailoring agents or in some cases, facet-dependent synthesis (for *e.g.* in case of BiOCl), or introducing some structural defects.[11,13] The work of Adriana *et al.* on the effect of different synthesis conditions on the photocatalytic activity of BiOCl show significant findings.[14] The author reported the removal of gallic acid by BiOCl and further describes the dependence of physicochemical properties and photocatalytic efficiency of BiOCl on the synthesis temperature conditions. This shows how changes in synthesis conditions can have substantial effect on the overall performance of a photocatalyst.

Talking about crystallization factors influencing the photocatalytic behavior of the photocatalyst, some other parameters that can affect the properties of a photocatalyst is the addition of compounds that acts as a modifier. For instance, addition of carbonaceous materials (for *e.g.* carbon nanotubes-CNTs). For long, CNTs have benefitted several photocatalysts, including TiO_2 and Bi-based photocatalysts, in terms of extending their light-harvesting response from UV to visible light region.[15,16] CNTs due to their good electrical conductivity and adsorption of reactants, acts as an electron sink or as a photosensitizer. For instance, in a study of multiwalled carbon nanotube, TiO_2 and Ni composite catalyst (MWNT–TiO_2:Ni) by Ou and coworkers, MWCNT acted as a photosensitizer by absorbing the light and transporting the photogenerated electrons into the conduction band of TiO_2 particles and further to isolated Ni particles which reduced the water molecules to H_2.[17] By virtue of their high specific surface area, hollow layered structure and presence of delocalized π-electrons, CNT facilitated in enhancing light absorption capacity and charge transportation phenomena. They are known to accelerate the electron transfer and thereby suppressing the recombination process. Nonetheless, this is not always the case. For instance, in our previous study of BiOBr/CNT composites, we observed that CNT was not contributing fully to the high photocatalytic activity for phenol rather other factors were dominant in some cases and suppressed the action of CNTs.[18] Our research group has also studied the optimal content of MWCNT in TiO_2/MWCNT composite that resulted in enhanced photodegradation of both phenol and oxalic acid.[19] Similarly, several other reports in literature could be found on effect of MWCNT on overall photocatalytic efficiency of BiOX[19,20].

Until now, none of the reports so far has ever reported any kind of correlations between the CNTs amount, structural and optical properties of BiOCl with its overall photodegradation efficiency. In this work, we have synthesized composites of BiOCl with CNT and further studied the influence of three key factors, crystallization temperature, time and CNT amount on the physicochemical properties of BiOCl/CNT composite. Based on the results, different correlations were made. Further, we have investigated the effect of CNTs on the overall photocatalytic efficiency of BiOCl/CNT composites for the removal of phenol under UV and rhodamine B (RhB) under visible light irradiation.

2. Experimental

2.1. Materials

Bismuth nitrate pentahydrate [Bi $(NO_3)_3 \cdot 5H_2O$] (Sigma-Aldrich, 98.0%), glacial acetic acid (Molar Chemicals Ltd., 100%), potassium chloride (Molar Chemicals, 99.7%), functionalized carbon nanotubes (Nanothinx S. A., Greece), Phenol (VWR extra pure, 100%) and RhB from Alfa Aesar (no purity data given). All the reagents were of analytical grade and used without further purification. Deionized water was used for the entire study. Methanol of HPLC-grade was used for HPLC measurements to prepare the necessary eluent for the analysis.

2.2. Methods

Synthesis of BiOCl and BiOCl/CNT composites. In the synthesis, two solutions (A and B) were used. For solution A, 3 g $Bi(NO_3)_3 \cdot 5H_2O$ was dissolved in 3 mL glacial acetic acid under continuous magnetic stirring and heated to ~45 °C to speed up the solubilization process. After this, a clear solution was obtained and thereafter the calculated amount of CNTs were added followed by 25 mL of deionized water and the suspension was ultrasonicated for an hour. The desired composition of CNTs in BiOCl were made 0.5 wt%, 1 wt% and 2 wt%. For solution B, 0.46 g of potassium chloride was dissolved in 25 mL deionized water and mixed thoroughly. Then, solution B was added dropwise to solution A under continuous magnetic stirring. The mixture was stirred for another 30 minutes. A white-colored suspension was obtained which was then transferred to a 120 mL Teflon-lined® stainless-steel autoclave and subjected to the desired heat treatments at different temperatures (120 °C & 150 °C) and time intervals (4.5 hours and 6.5 hours, in both cases of temperature values). The mixture was then cooled down naturally to room temperature and the product was collected and washed with ethanol and deionized water, three times each and dried in an oven around 40 °C overnight.

For the synthesis of BiOCl reference samples (without CNTs), the process was same as described above. The total number of samples prepared were 16, out of which 4 were the reference sample BiOCl (one each from different synthesis conditions) and rest 12 were composites with CNT (BiOCl/CNT).

2.3. Characterization

The samples were characterised using X-ray diffraction to study the phase compositions and crystal orientations. A Rigaku Miniflex II diffractometer, X-ray diffraction, with the following measurement conditions was used: $2\theta^\circ = 10$–80°, λ (Cu Kα) = 0.15406 nm, 40 kV and 30 mA. The primary crystallite size (d) was calculated by using following well-known Scherrer equation:

$$d = k\lambda \div \beta \cos\theta$$

where, k is the shape factor constant, usually in the range of 0.8–1.2 (typically taken value is 0.9, in case of spherical particles or if shape information is unknown), λ is the X-ray wavelength, θ is the Bragg angle and β is the peak width at full width at half maximum intensity (FWHM) of the peak in radians, also known as line broadening and can be calculated as $\beta = \beta_s - \beta_0$, where β_s and β_0 are XRD peak half-widths of the sample and of the silicon standard.

Morphological analysis was carried out using Scanning Electron Microscopy (SEM), Hitachi S-4700 Type II SEM and Transmission Electron Microscopy (TEM). During SEM measurements, the electron beam was produced using a cold field emission gun applying 10 kV acceleration voltage. For TEM measurements, the as-prepared samples were examined by high-resolution transmission electron microscopy (HRTEM, FEI Tecnai G2 electron microscope, 200 kV) to explore the morphology and particle size of the nanocomposites. Sample preparation was made by dropping an aqueous suspension of the nanocomposites on 300 mesh copper grids (lacey carbon, Ted Pella Inc.). N_2 adsorption–desorption measurements were carried at 77 K using a BELCAT-A device to measure the specific surface areas of the samples and calculations were done *via* BET (Brunauer–Emmett–Teller) method.

A Jasco-V650 spectrophotometer with an integration sphere (ILV-724) was used for measuring the diffuse reflectance spectra of the samples ($\lambda = 220$–800 nm). The indirect band-gap energy was calculated using the Kubelka–Munk equation, that is $[F(R)\cdot\hbar\nu]\ p = A(\hbar\nu - E_g)$, where $\hbar$ is Planck constant, E_g is the band gap energy, A is constant and p is dependent on the type of optical transition and Tauc plot is used to determine the band gaps of the samples by plotting the graph between $(\alpha h\nu)^{1/2}$ *vs.* photon energy ($h\nu$).[21] In some cases, the possible electron transitions were evaluated by plotting the first derivative spectra $d\lambda\cdot dr^{-1}$ where λ is the wavelength and r is the reflectance.

2.4. Photocatalytic measurements

The photocatalytic activity of the composites was determined by measuring the photodegradation of phenol and RhB in an aqueous solution under UV-A, or visible light, respectively. The initial concentration taken for phenol and RhB (C_0) was 0.1 mM and 0.4 mM, respectively. For the test, the suspension containing the pollutant and photocatalyst were continuously purged with air to keep the dissolved oxygen concentration constant throughout the experiment. In case of UV-A irradiation, 6 × 6 W fluorescence UV-A lamps (Lightech, Dunakeszi, Hungary) with 365 nm emission maximum were used. For the visible light irradiation, 4 conventional energy saving lamps (Düwi 25920/R7S24W) were used. The amount of catalyst loaded was 1.0 g L^{-1} with 130 mL of the total volume of the suspension (V_{susp}). Initially, the suspension was ultrasonicated for about 5 minutes to ensure a homogeneous suspension for the experiment.

For phenol, the dark period to achieve the adsorption/desorption equilibrium was 30 minutes. The total irradiation time was 2 hours under UV-A irradiation. The samples were withdrawn in regular time intervals. The collected samples were then centrifuged (13 500 rpm min^{-1}) for 3 minutes and filtered with Filtratech 0.25 μm syringe filter. The decrease in the concentration of phenol was measured by HPLC (Merck-Hitachi L-7100) with a low-pressure gradient pump, equipped with a Merck-Hitachi L-4250 UV-vis detector and a Lichrospher R_p 18 column using a methanol/water (50 : 50 v/v) mixture as eluent and 210 nm as the detection wavelength.

For RhB, the dark period of the suspension was 10 minutes. The irradiation time in case of RhB was also same as in the case of phenol but under visible light irradiation and the same process was followed. The dye concentration was measured using UV spectrophotometer, JASCO-V650 at the maximum absorption wavelength of RhB, $\lambda_{max} = 553$ nm.

3. Results and discussions

3.1. Structural investigation of BiOCl/CNT composites

The crystal structure of pure BiOCl and BiOCl/CNT composites were investigated by X-ray diffraction (XRD) and the diffractograms of the samples are shown in Fig. 1(a and b). All the diffraction peaks can be indexed to tetragonal structure of BiOCl (JCPDS 06-0249). The peaks at 12.17°, 24.1°, 25.92°, 32.50°, 33.29°, 36.50°, 40.87°, 46.66°, 49.64°, 55.21°, and 58.60° correspond to the crystal planes of (001), (002), (101), (110), (102), (003), (112), (200), (113), (211) and (212). All of the other samples showed similar diffraction patterns. The characteristic peaks for CNTs were absent in all the cases probably due to its low amount and overlapping with the diffraction peak of (101) crystal facet of BiOCl. As it can be seen from the diffractograms, the composites showed similar diffraction peaks as that of its reference sample (bare BiOCl), therefore, it could be suggested that no change in the structure of BiOCl occurred with the introduction of CNTs. However, a little variation in the relative intensity values of the peak profiles can be seen among different sample series. Interestingly, compared to the standard diffraction pattern (JCPDS: 06-0249), the diffraction peak intensity of (102) plane, in all cases, is relatively stronger than that of the other planes and in some situation, the diffraction peak of (001) was missing, as shown in Fig. 1(b). Additionally, the literature has reported mostly (101) or (110) as the dominant crystallographic planes but in our study, the preferred orientation is along (102) for all the sample series.[22] Clearly from the diffractograms, higher crystallinity could be seen in case of

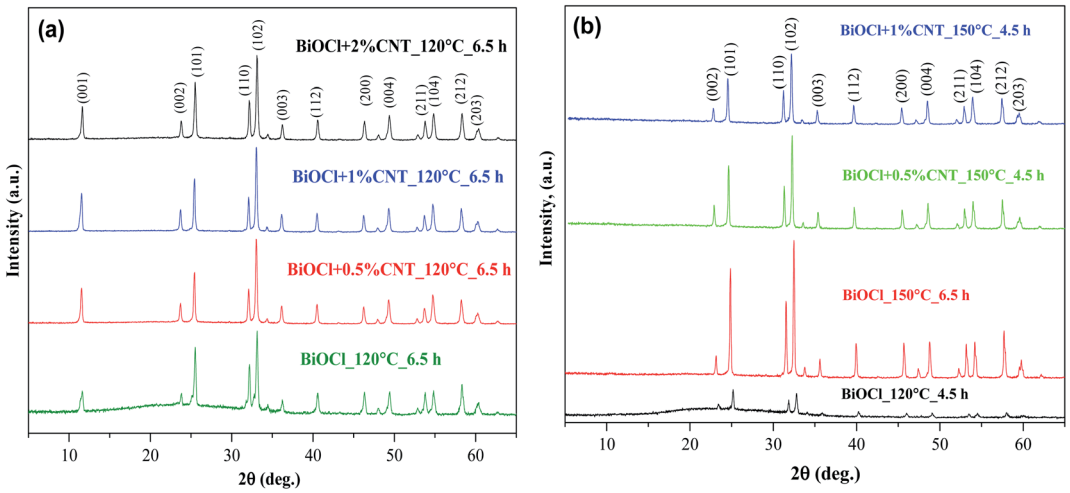

Fig. 1 XRD patterns of samples showing reflections of (a) BiOCl/CNT composites prepared at 120 °C for 6.5 h (b) BiOCl/CNT composites showing absence of (001) crystallographic plane.

samples containing CNTs and was also reported elsewhere[23] and in our previous studies of BiOBr/CNT and BiOI/CNT.[18,24] From Fig. 1(a and b), it is evident that a larger portion of amorphous region is present in case of the reference samples (pure BiOCl). Besides CNT amount, higher temperature conditions have also contributed to the high crystallinity of the samples. For instance, at high temperature condition (150 °C), the reference samples were also crystalline and the amorphous region was absent unlike in the case of 120 °C, also visible in Fig. 1(a). This indicates that presence of CNT and use of higher hydrothermal crystallization temperature is enhancing the overall crystallinity of the materials.

The primary crystallite size was also calculated for the samples using the Scherrer equation as discussed in the experimental section. Through the calculations, it was observed that the primary crystallite size of the samples prepared at 120 °C were comparatively lower than that of the samples prepared at 150 °C. This is a common phenomenon because generally higher temperature condition leads to larger crystal formation. At 150 °C, a wider variation in crystallite size was observed. For example, the primary crystallite size ranged approximately between 40–125 nm in case of 150 °C while those synthesized at 120 °C were in between 60–80 nm. Although there is a wider range in the primary crystallite size of the samples at 150 °C but a clear sharp decrease was observed with increasing CNT content which means that CNTs are also affecting the primary crystallite size of the composites besides crystallinity. The range of crystallite size for the composites prepared at 150 °C is represented in Table 1. The crystallite values above 100 nm obtained from the Scherrer equation calculation does not represent a precise value and therefore, we have represented those values in an approximate value.

3.2. Morphological investigation of BiOCl/CNT composites

In order to study the influence of CNT and hydrothermal synthesis conditions on morphology, the samples were measured using TEM and SEM. BiOCl/CNT composites displayed mostly irregular, non-hierarchal structure of micro-sheets. All the samples have the similar morphology. The Fig. 2(a–c) is the representative image concerning BiOCl and BiOCl/CNT samples. Fig. 2(b and c) shows the stacking of these micro-sheets. In addition to this, the surfaces of these sheets were extremely smooth while no pores could be seen on its surface. It is quite common to see the aggregation of nano/microsheets of BiOX when the synthesis involves aqueous media, as discussed previously in ref. 2 and this is why it could be the reason of the aggregation of microsheets in our study. For this reason, some authors have reported the use of ionic liquids during the synthesis to avoid random aggregation of individual nanoplates/sheets.[25] On the other hand, in case of CNT-containing samples, as the amount of CNT increased, the irregular shaped nanoplates started to build edges at the corners creating a uniform square-like nanoplates, shown in the inset of Fig. 2(d). This square-like morphology was also observed in a study by Xiong *et al.* where the author used mannitol as a template-directing agent which resulted in the formation of such square-like BiOCl nanoplates.[26] However, this distribution of square-like nanoplates was, of course, not homogeneous in our case. Also, these changes were not significantly dependent on synthesis parameters (time and temperature).

Table 1 Variation in primary crystallite size as a function of CNT in the BiOCl and BiOCl/CNT composites prepared at 150 °C

Sample names prepared at 150 °C	Primary crystallite size (in nm)
BiOCl_150_4.5 h	**>100**
BiOCl + 0.5%CNT_150_4.5 h	>100
BiOCl + 1%CNT_150_4.5 h	~89
BiOCl + 2%CNT_150_4.5 h	**42.5**
BiOCl_150_6.5 h	**>100**
BiOCl + 0.5%CNT_150_6.5 h	>100
BiOCl + 1%CNT_150_6.5 h	~94
BiOCl + 2%CNT_150_4.5 h	**43.3**

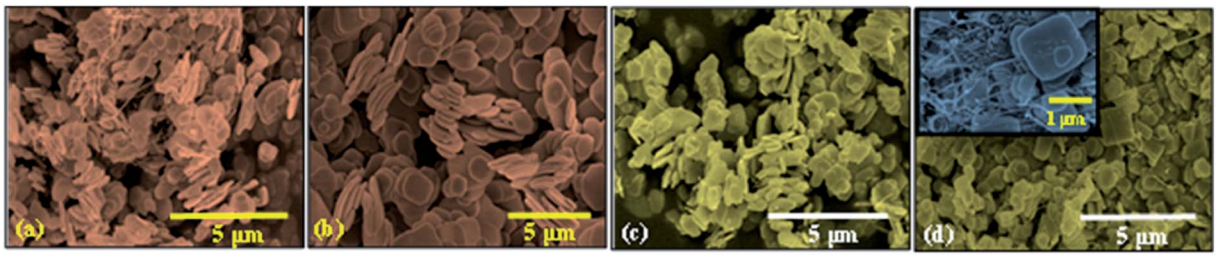

Fig. 2 SEM micrographs of BiOCl and its composites with CNT (a) BiOCl + 0.5% CNT_120 °C_6.5 h (b) BiOCl_150 °C_4.5 h (c) BiOCl + 0.5% CNT_120 °C_4.5 h (d) BiOCl + 2% CNT_120 °C_4.5 h.

In addition to this, the authors also conducted TEM and HRTEM measurements for pure CNT and BiOCl/CNT composite to gain the better understanding of CNT interactions and the defects created by them. Fig. 3(a) represents SEM micrograph of pristine CNT. Fig. 3(b) shows the TEM image of pristine CNT and in order to examine the presence of CNT and its defect sites, HRTEM analysis was also conducted, as can be seen in Fig. 3(c). In these images, the uniform structure with rather smooth and very well graphitized parallel walls of pure CNT could be observed. The functional groups on CNT's surface are correlated to defect sites in several studies and presence of such defects on the semiconductor photocatalyst material have positive influence on the affinity bonding of CNT to other particles and in charge transfer process during photodegradation phenomena. In our work we used MWCNT produced by the CVD technique and we know that those exhibit a higher quantity of structural defects due to their multiple graphite layers and intershell structural defects. Fig. 3(d) shows TEM image of BiOCl/CNT composite and the existence of CNT is observed in the TEM image and the heterogeneous distribution of CNT on BiOCl microplates could also be seen. The tube-shaped material on right side of the same image are the CNTs and the dark regions reflects the overlapped BiOCl microplates with average crystallite size of <70 nm, as calculated by the Scherrer equation (see XRD section).

3.3. Optical investigation of BiOCl/CNT composites

The optical properties of the composites were studied by using diffuse reflectance spectroscopy. The band gap values of BiOCl and BiOCl/CNT composites were calculated and it fall in the range of 2.96–3.38 eV. Fig. 4(a) shows the DRS spectra of the composites prepared at 120 °C for 6.5 h. The absorption maximum for BiOCl was observed around ~353 nm. This suggests that the samples have strong light absorption in the UV region. Through the first derivative of the DRS spectra, as shown in Fig. 4 (b), it was found that the addition of CNT led to the blue shift in the absorption edge maxima. Similar blue-shift was also observed with increasing CNT amount in BiOI in another study.[27] This means that the emission and excitation bands are different. Additionally, the composites showed a decrease in the band gap values. In case of samples without CNT, the band gap was in between 3.26–3.38 eV while for composites the band gap values fall in a much wider range between 2.96–3.15 eV, depending on the amount of CNT and synthesis conditions. The decrease in the band gap of composites with CNT was also reported in ref. 28. These identical results could be explained through the previous reports which dealt with the influence of CNT on the optical properties of a photocatalyst. One of it explains the photosensitizer behavior of CNT that is responsible for extending the spectral spectrum for photocatalyst.[29] Also, it is assumed that the presence of covalent bonding between the photocatalyst and CNT can even contribute to extended light absorption. We assume similar phenomenon of enhanced light absorption occurred in our study as well after the incorporation of MWCNT.

3.4. Photocatalytic evaluation

The photocatalytic efficiency of the samples was demonstrated for the removal of pollutants, RhB and phenol, under visible and UV light, respectively. The samples were tested for aqueous solution of both the pollutants. In case of RhB

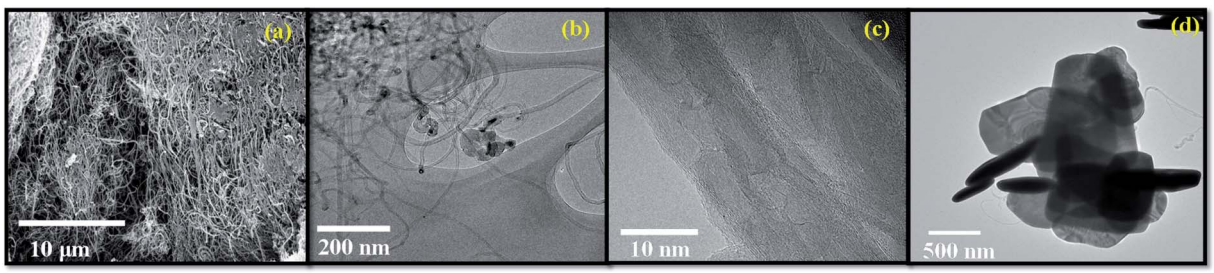

Fig. 3 (a) SEM micrograph of pure CNT (b) TEM image of pristine CNT (c) HRTEM of pristine CNT representing graphitic sheets that corresponds to the defect sites due to the presence of functional groups on CNTs surface (d) TEM image of BiOCl/CNT composite prepared at 120 °C for 4.5 h.

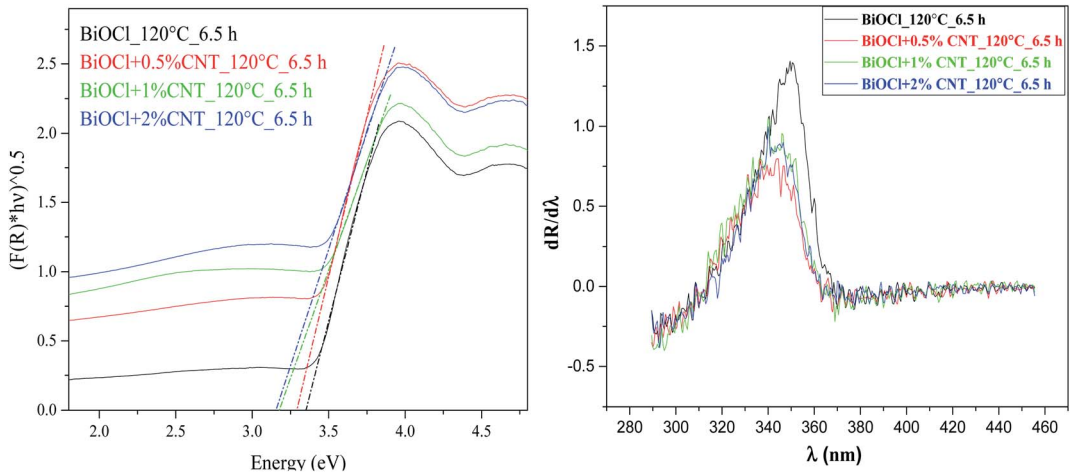

Fig. 4 Plots of $(\alpha h\nu)^{1/2}$ *versus* $h\nu$ BiOCl/CNT composites prepared at 120 °C at 6.30 h showing band gap values (on the left) first derivative spectra (on the right).

photodegradation, complete removal with the maximum degradation efficiency of 98% was achieved by pure BiOCl prepared at 120 °C for 6.5 h and the solution became transparent after 120 minutes of irradiation. Even though this sample contains background of amorphous region, as evident from XRD, higher photocatalytic activity was observed. This indicates the role of other factors contributing in the photodegradation process which will be discussed later. Considering the composites, the minimum degradation efficiency of 52% and maximum of 88% RhB removal rates were obtained under visible light irradiation, shown in Fig. 5. Both of these samples belong to the similar sample group, *i.e.* at 120 °C for 6.5 h, represented in Fig. 5. From the figure, it is clear that almost 20% of the adsorption took place and rest of the dye was photocatalytically removed. In spite of having wide band gap, BiOCl can efficiently degrade RhB under visible light irradiation. This is, apparently, due to the phenomenon called "indirect dye photosensitization" process, where the dye molecule gets excited and transfers the photo-excited electron to the conduction band of semiconductor.[30,31] This could possibly be the reason of photocatalytic activity of BiOCl for RhB under visible light irradiation.

Among the composites with different CNT contents, the sample with 0.5% CNT prepared at 120 °C for 6.5 h showed the maximum degradation efficiency of 88% for RhB as stated above under visible light irradiation in 120 min. For the rest of the samples, the removal efficiency ranged in between 60–83%. Fig. 6 shows the trend observed in the photocatalytic degradation of RhB as a function of CNT amount under visible light. It is clear from Fig. 6 that the composites with 0.5% and 2% CNT are showing the similar pattern for photodegradation efficiency (% deg.) as a function of CNT amount. However, no specific trend can be seen for 1% CNT and without CNT samples. This suggests that difference in the photocatalytic activity in the latter case cannot be directly correlated to CNT amount.

To better elucidate the performance of the composites, the photocatalytic activity of the samples were compared by using a colorless pollutant (phenol). Since phenol is colorless, the photosensitization process does not occur. Additionally, phenol is a weakly adsorbing compound on the surface of several catalysts.[32] Due to the wide band gap of BiOCl, no photocatalytic activity was observed for phenol under visible light. The degradation efficiency of the sample was in the range between 30–45% under UV-A irradiation. These values represent promising values in the areas of removal of such recalcitrant pollutants since ordinary lamps were used in this study. The samples prepared at higher temperature and longer heat treatment conditions (at 150 °C for 6.5 h) showed the maximum removal efficiency for phenol under UV light. Fig. 7 shows the concentration changes in phenol over time by the samples prepared at 150 °C for 6.5 h with different CNT content. This is the best performing sample series among all and so we represented these samples here. In order to compare the results more efficiently, the photodegradation efficiencies of the samples were compared with respect to CNT amount (Fig. 7). As observed in Fig. 6, the same compositions (0.5% and 2% CNT) showed trends similar to each other. In addition to this, pure BiOCl samples also showed some relatable trends to 0.5% and 2%

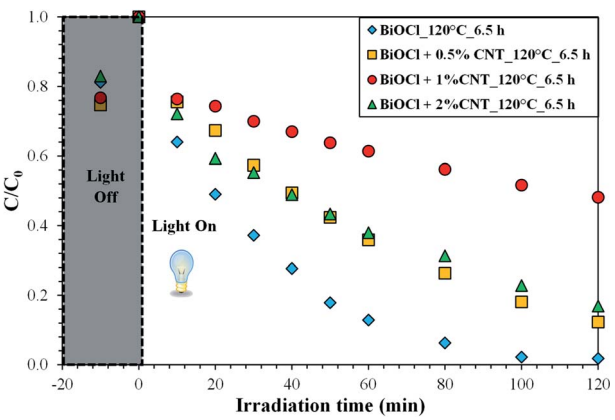

Fig. 5 Photodegradation efficiency of BiOCl and BiOCl/CNT composites prepared at 120 °C_6.5 h for RhB under visible light irradiation.

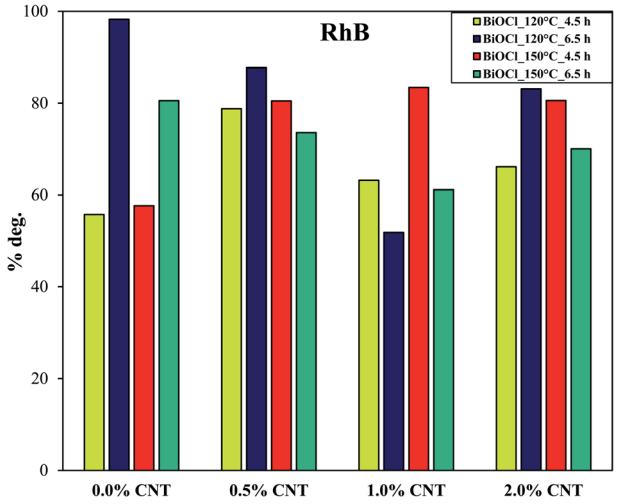

Fig. 6 Trend reflecting the % photodegradation of RhB by BiOCl and BiOCl/CNT composites under visible light as a function of %CNT.

CNT composites. The composition with 1% CNT again did not show any specific trend. When the amount of CNT was high (2%), the photocatalytic activity was also high under UV light irradiation. Even lower CNT amount (0 or 0.5%) showed higher photodegradation efficiency in some cases while most of the samples with medium CNT amount (1% CNT) experienced lower photocatalytic activity. Now here arise several questions which could be answered if some correlations could be made. Therefore, our next step was to find some connections between the photocatalytic activity and physico-chemical properties of the samples.

3.5. Linking the photocatalytic activity to the investigated properties

Several correlations were explored to see the dependence of photocatalytic activity on the physico-chemical properties of the BiOCl and BiOCl/CNT composites. For this, two parameters were selected which were structural and optical properties since

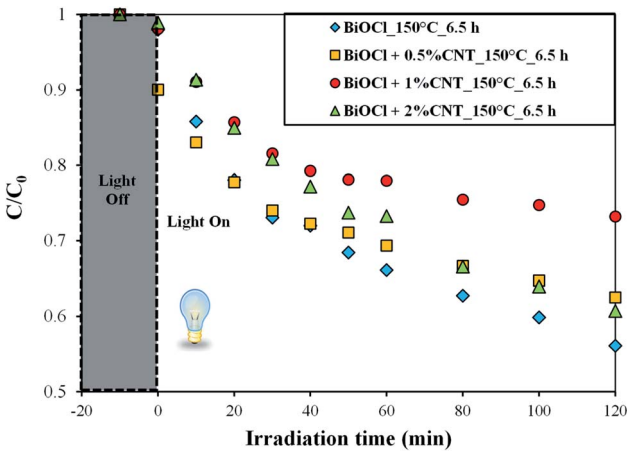

Fig. 7 Photodegradation efficiency of BiOCl and BiOCl/CNT composites prepared at 150 °C_6.5 h for phenol under UV-A irradiation.

the results from XRD and DRS gave some hints. In our previous studies also, some interesting correlations were found such as those with the photocatalytic activity and band gap energy. For instance, our previous report on BiOI/CNT shows a clear dependence of photocatalytic performance of the composites on the band gap energy where the samples with higher band gap energy showed the lowest photocatalytic activity.[24] However, our other previous study on BiOBr/CNT showed opposite trend where higher photocatalytic activity was found for samples with higher band gap energy.[18] Therefore, we wanted to see if any interesting correlations that could be seen for our BiOCl and BiOCl/CNT composites. Unlike the results of our previous studies, no significant correlation could be made with band gap energy in this study. Nonetheless, we could see a clear and important relation with the structural properties (primary crystallite size) of BiOCl with their photocatalytic activity. For BiOCl and BiOCl/CNT composites, the crystallite size seems to affect the overall photocatalytic activity. The samples with higher crystallite size showed higher photocatalytic activity which was also observed in our BiOBr/CNT study.[18] Generally, the higher crystallite size means lower specific surface area that means lower number of active sites and thus lower photocatalytic performance – although the surface normalized values could be higher.[33] Here, we found that the samples with larger primary crystallite size showed higher photocatalytic performance and were among the best samples for phenol degradation. The crystallite size is, therefore, one of the important parameter to consider as it can influence the photocatalytic activity although its effect varies depending on the type of halogen in bismuth oxyhalides. Therefore, in the subsequent section we will discuss in detail about its effect on our BiOCl and BiOCl/CNT composites.

3.6. Crystallite size *vs.* photocatalytic activity

In this section, we tried to correlate the CNT amount and synthesis conditions with the primary crystallite size and further its influence on their photodegradation efficiency. At lower temperature and shorter period of crystallization (120 °C, 4.5 h), a narrow range of crystallite size was seen, as shown in Fig. 9 (marked in green and blue). As more and more energy was applied to the samples (150 °C, 4.5 and 6.5 hours), an enlarged spectrum of crystallite size was observed, shown in Fig. 9 (marked in red and purple). This shows that the spectrum of crystallite size grew with rise in hydrothermal crystallization temperature which was enough for CNT to impart crystallinity and take part in charge distribution process. This means that enough time and temperature was given to the crystals for their growth and thus higher crystallization was seen in the samples and *vice versa*. This is why the samples with lower or no CNT amount (0.5 or 0%), see Fig. 9 (top right), with larger crystallite size and lower crystallinity also showed higher photocatalytic activity because the hydrothermal crystallization conditions (time and temperature) are playing a crucial role.[34] It indicates that at lower CNT amount, hydrothermal crystallization conditions are one of the prime or controlling-factor in deciding the photocatalytic performance of BiOCl/CNT composites.

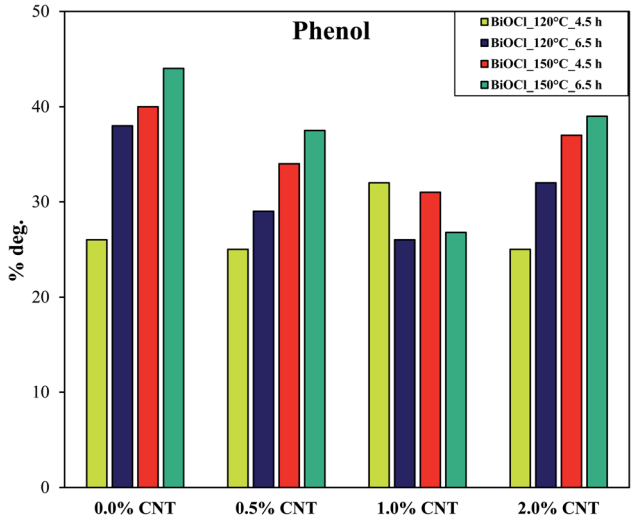

Fig. 8 Trend reflecting the degradation efficiency of phenol by BiOCl and BiOCl/CNT composites under UV-A irradiation as a function of % CNT.

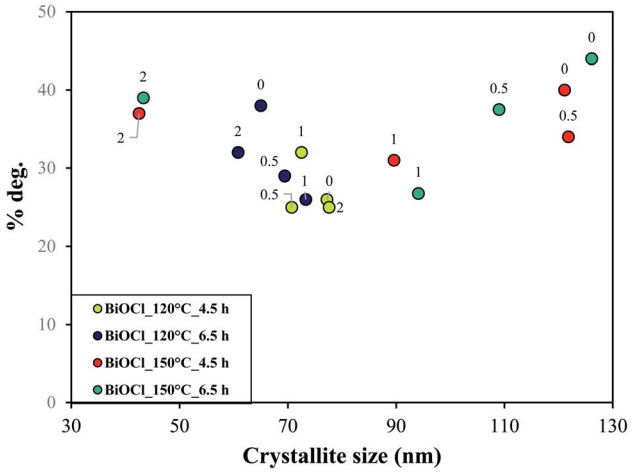

Fig. 9 Correlation between crystallite size and photodegradation efficiency of BiOCl and BiOCl/CNT composites for phenol under UV light synthesized at different hydrothermal conditions and containing varying amount of CNTs (0.5, 1, 2 wt%).

However, samples with higher CNT amount (2%) also shows maximum photodegradation efficiency (top left in Fig. 9) which again indicates that there are other factors also which are influencing the photocatalytic activity of the composites. Therefore, we made different correlation with the optical properties, %CNT and crystallinity.

When no direct relation was seen with the band gap energy and the photodegradation efficiency, we compared the first derivative spectra (absorption maximum) of the samples with their photocatalytic activity. Some interesting connection was found, as shown in Fig. 8. At higher percentage of CNT (2% CNT), the dependence on excitability was observed, however, at lower percentage (0, 0.5 and 1% CNT) no dependence on optical properties was found. At this point, it was an indication for us that there exists a relation between CNT amount and optical properties of our material. Therefore, we made correlation between the absorption maxima and degradation efficiency of samples, see Fig. 10. Lower CNT amount (0.5 and 1%) did not show any specific trend and so does not seem to interfere with the optical properties of our BiOCl/CNT material, although lowering of band gap was observed in case of composites but then again it did not show any correlation with the photocatalytic activity. This is why it is not represented here. Out of all, the most relevant and significant relation was chosen and represented which included samples containing higher CNT amount (2%). These composites exhibit red-shift (which is still in the UV region due to the wide band gap of BiOCl). As a result, these samples witnessed higher photocatalytic activity which means CNT interferes with the charge distribution process at this amount. Considering Fig. 10, as the crystallization conditions favored higher crystallinity, red shift appeared in the samples with increasing hydrothermal crystallization temperature and time which further resulted in higher photocatalytic activity.

It is evident from Fig. 9 that the samples on the left are the ones with least crystallinity (proved through XRD) which increases as we go up with higher hydrothermal temperature and time conditions. The least crystalline material among this has the higher crystallite size and therefore, lower surface properties and showed lowest photocatalytic activity and *vice versa*. This correlation shows that there is an interaction between the optical and structural properties of the semiconductor material and CNTs at a specific concentration.

From Fig. 9 and 10, important conclusions can be made related to CNT amount and hydrothermal crystallization temperatures on BiOCl photocatalytic performance. As evident from the results, 1% CNT did not show any clear relation in response to optical or structural properties and photocatalytic activity. Nonetheless, lower CNT amount showed dependency on structural properties (primary crystallite size) and higher CNT amount on optical properties (absorption wavelength). Moreover, the amount of CNT cannot be considered as the sole or main reason for enhanced photocatalytic performance of BiOCl/CNT (2%) composites. This is for the simple reason that

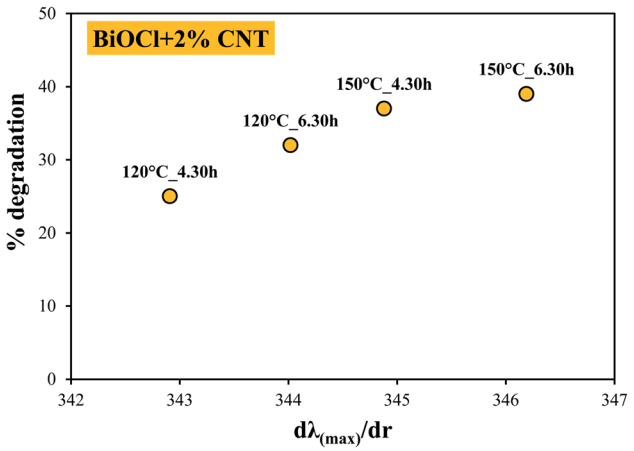

Fig. 10 Correlation between the absorption maximum and degradation efficiency of BiOCl + 2% CNT composites showing dependence on excitation wavelength.

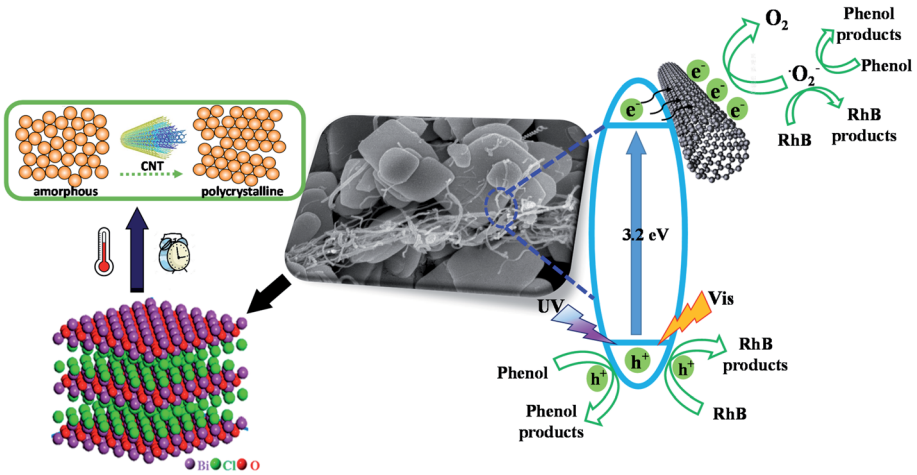

Fig. 11 Schematic illustration of different events occurring during the hydrothermal crystallization and photocatalytic degradation of phenol and RhB under UV and visible light irradiation, respectively.

sufficient energy is required for CNT to play a role in the charge separation phenomena and to enhance the photocatalytic performance of semiconductor materials like BiOCl. These correlations gave us a fundamental understanding of the materials belonging to bismuth oxyhalide family. Our studies have shown that different trends and dependency could be seen for one member of BiOX which may or may not be true in the case of other member of BiOX family.

3.7. Proposed mechanism

From Fig. 6, some interesting observations were found with respect to the amount of CNT and hydrothermal synthesis conditions. As can be seen from Fig. 6 that in case of reference samples (0% CNT), when the crystallization time is short, the process of crystallization of the crystals did not complete and hence, not sufficient time was given for the crystal to grow which would be favorable for photocatalytic performance. As a result, some amorphous region is still present with low crystallinity but when enough time was given, higher crystallinity was attained. Therefore, even though when there are no CNTs, the samples show significant photodegradation of RhB under visible light irradiation. This indicates here that the duration of hydrothermal crystallization was very effective in enhancing the photocatalytic performance of the BiOCl samples. When CNT was present, its positive effect on crystallization was visible in some cases. Contrary to this, the activity enhancing role of CNTs get suppressed in other cases due to hydrothermal crystallization conditions which means higher hydrothermal time and temperature are sufficient for proper crystal formation even without the presence of CNT. This is why we cannot see the clear trend for samples with different CNT compositions. This shows that these parameters (time, temperature and CNT amount) compete with each other for gaining effective crystallization. In case of phenol photodegradation, Fig. 8 shows that in all cases the beneficial effect of CNTs was suppressed due to hydrothermal crystallization. For reference samples it is clear that increasing both time and temperature is beneficial for phenol degradation most probably because of higher crystallinity. The same trend can also be observed for the samples containing CNT, except for 1% CNT.

The difference in photocatalytic activity of RhB and phenol can be explained by two facts. One is the adsorbability of the two model pollutants: it can be presumed that CNT can enhance adsorption of RhB in certain cases (short hydrothermal time) thus trapping the organic compound on the surface which then can migrate to the photocatalytically active sites. The other reason might be the possible photosensitizing effect which helps in harvesting the energy of visible light *via* RhB adsorption even in the presence of a semiconductor having relatively high band gap (with higher crystallinity of BiOCl these effects are suppressed). The pictorial representation of this can be seen in Fig. 11. The investigation concerning the intermediates and end-products during the photocatalytic process is quite complex and requires a separate study on its own. Therefore, it is not included in this study.

4. Conclusions

In the present study, the composites of BiOCl with CNT were synthesized *via* hydrothermal method. Various compositions of CNT and different synthesis conditions were applied. Microplates-like morphology was obtained for the samples without CNT while in presence of CNT, edges started to appear forming a square-like morphology. This shows that addition of CNT led to some morphological changes in BiOCl. The crystallinity of the composites was enhanced with increasing amount of CNT. The higher degree of crystallization was also observed when higher temperature and longer duration was applied during the synthesis. The primary crystallite size of the composites experienced a sharp decrease with increasing CNT content. The optical properties of the composites were also affected by the presence of CNT. A decrease in the band-gap of composites was seen. The photocatalytic activity of pure BiOCl reported almost 98% removal of RhB under visible light and

more than 40% of phenol photodegradation under UV-A light irradiation. This study forms the fundamental for the materials like CNT that acts as a crystallinity promoter. Through the results obtained in this study, it can be interpreted that such nanostructures can promote higher photocatalytic activity to the photocatalyst, under certain circumstances, even if the semiconductor material loses its surface properties during the hydrothermal crystallization treatment. In other words, using electron conductive materials like CNTs in appropriate concentration could compensate the loss of surface properties of the material by enhancing its photocatalytic activity. This could be due to its influence on the optical properties of the material. This study also illustrates that if a crystalline semiconductor material is present, CNT can facilitate the photocatalytic process by interacting with it. On the contrary, at lower CNT amount, the crystallite size becomes more predominant and a deciding-factor when it comes to the superior performance of BiOCl/CNT composites.

Conflicts of interest

There are no conflicts to declare.

Acknowledgements

This work was supported by the Indo-Hungarian TÉT project (TÉT_15_IN-1-2016-0013) and Department of Science and Technology, Delhi, India (INT/HUN/P-06/2016). The authors would like to acknowledge the financial support received from Bilateral Scholarship, Tempus Public Foundation, Hungary. Special thanks to my colleagues, Szilvia Fodor, Gyulavari Tamas, Kovacs Gabor for carrying out SEM and DRS measurements. This research was supported by the European Union and the Hungarian State, co-financed by the European Regional Development Fund in the framework of the GINOP-2.3.4-15-2016-00004 project, aimed to promote the cooperation between higher education and the industry.

References

1 R. He, S. Cao, P. Zhou and J. Yu, *Cuihua Xuebao*, 2014, **35**, 989–1007.
2 J. Li, Y. Yu and L. Zhang, *Nanoscale*, 2014, **6**, 8473–8488.
3 K. L. Zhang, C. M. Liu, F. Q. Huang, C. Zheng and W. D. Wang, *Appl. Catal., B*, 2006, **68**, 125–129.
4 C. Zhao, F. Xu, L. Sun, J. Chen, X. Guo, E. Yan, F. Yu, H. Chu, H. Peng, Y. Zou, Z. Liu and F. Li, *Int. J. Hydrogen Energy*, 2019, **44**, 6655–6662.
5 Y. Zhao, T. Chen, R. Ma, J. Du and C. Xie, *Micro Nano Lett.*, 2018, **13**, 1394–1398.
6 K. Li, Y. Liang, J. Yang, Q. Gao, Y. Zhu, S. Liu, R. Xu and X. Wu, *J. Alloys Compd.*, 2017, **695**, 238–249.
7 M. Kah, H. Walch and T. Hofmann, *Environ. Sci.: Nano*, 2018, **5**, 882–889.
8 W. Wu, Y. Song, L. Bai, Z. Chen, H. Sun, G. Zhen, R. Zhan, Y. Shen, J. Qian, Q. Yuan and Z. Sun, *ACS Appl. Nano Mater.*, 2020, **3**, 9363–9374.
9 J. Liao, K. Li, H. Ma, F. Dong, X. Zeng and Y. Sun, *Chin. Chem. Lett.*, 2020, **31**, 2737–2741.
10 H. Chen, X. Yu, Y. Zhu, X. Fu and Y. Zhang, *J. Nanopart. Res.*, 2016, **18**, 1–13.
11 E. Bárdos, A. K. Király, Z. Pap, L. Baia, S. Garg and K. Hernádi, *Appl. Surf. Sci.*, 2019, **479**, 745–756.
12 D. Qian, S. Zhong, S. Wang, Y. Lai, N. Yang and W. Jiang, *RSC Adv.*, 2017, **7**, 36653–36661.
13 E. Bárdos, A. K. Király, Z. Pap, L. Baia, S. Garg and K. Hernádi, *Appl. Surf. Sci.*, 2019, **479**, 745–756.
14 A. C. Mera, C. A. Rodríguez, L. Pizarro-Castillo, M. F. Meléndrez and H. Valdés, *J. Sol-Gel Sci. Technol.*, 2020, **95**, 146–156.
15 S. Yin, J. Di, M. Li, W. Fan, J. Xia, H. Xu, Y. Sun and H. Li, *Clean: Soil, Air, Water*, 2016, **44**, 781–787.
16 K. Hemalatha, P. M. Ette, G. Madras and K. Ramesha, *J. Sol-Gel Sci. Technol.*, 2015, **73**, 72–82.
17 Y. Ou, J. Lin, S. Fang and D. Liao, *Chem. Phys. Lett.*, 2006, **429**, 199–203.
18 N. Sharma, Z. Pap, S. Garg and K. Hernádi, *Appl. Surf. Sci.*, 2019, **495**, 143536.
19 B. Réti, K. Mogyorósi, A. Dombi and K. Hernádi, *Appl. Catal., A*, 2014, **469**, 153–158.
20 P. Gao, Z. Yin, L. Feng, Y. Liu, Z. Du, Z. Duan and L. Zhang, *Environ. Res.*, 2020, **185**, 109468.
21 P. Kubelka and F. Munk, *Zeitschrift für Technische Physik*, 1931, **12**, 593–601.
22 L. Wang, D. Lv, F. Dong, X. Wu, N. Cheng, J. Scott, X. Xu, W. Hao and Y. Du, *ACS Sustainable Chem. Eng.*, 2019, **7**, 3010–3017.
23 F. Gao, D. Zeng, Q. Huang, S. Tian and C. Xie, *Phys. Chem. Chem. Phys.*, 2012, **14**, 10572–10578.
24 N. Sharma, Z. Pap, I. Székely, M. Focsan, G. Karacs, Z. Nemeth, S. Garg and K. Hernadi, *Appl. Surf. Sci.*, 2021, **565**, 150605–150616.
25 A. Phuruangrat, S. Thongtem and T. Thongtem, *Appl. Phys. A: Mater. Sci. Process.*, 2020, **126**, 1–8.
26 J. Xiong, G. Cheng, G. Li, F. Qin and R. Chen, *RSC Adv.*, 2011, **1**, 1542–1553.
27 M. Su, C. He, L. Zhu, Z. Sun, C. Shan, Q. Zhang, D. Shu, R. Qiu and Y. Xiong, *J. Hazard. Mater.*, 2012, **229–230**, 72–82.
28 D. Liu, J. Xie and Y. Xia, *Chem. Phys. Lett.*, 2019, **729**, 42–48.
29 S. M. Lam, J. C. Sin, A. Z. Abdullah and A. R. Mohamed, *Fullerenes, Nanotubes, Carbon Nanostruct.*, 2014, **22**, 471–509.
30 L. Bao and Y. J. Yuan, *Dalton Transactions*, 2020, **49**, 11536–11542.
31 D. Zhang, J. Li, Q. Wang and Q. Wu, *J. Mater. Chem. A*, 2013, **1**, 8622–8629.
32 R. Kaveh and H. Alijani, *J. Asian Ceram. Soc.*, 2021, **9**, 343–365.
33 A. B. D. Nandiyanto, R. Zaen and R. Oktiani, *Arabian J. Chem.*, 2020, **13**, 1283–1296.
34 X. Wang, L. Sø, R. Su, S. Wendt, P. Hald, A. Mamakhel, C. Yang, Y. Huang, B. B. Iversen and F. Besenbacher, *J. Catal.*, 2014, **310**, 100–108.